First-principles study of hydroxyapatite surfaces and water adsorption

R. Astala* and M. J. Stott†
Department of Physics, Queen's University Kingston, Ontario, Canada K7L 3N6
(Received 26 August 2007; published 20 August 2008)

Hydroxyapatite (HA) is the main mineral component of natural bone and an important synthetic biomaterial. The surfaces of this material are critical as the biological action takes place at the interface between the HA and the biological medium. *Ab initio* total energy methods are used to study the atomic structure and surface chemistry of HA. Low index HA surfaces in vacuum, the adsorption of water on these surfaces, and the loss of Ca from them are considered. All surfaces are found to react strongly with water, and after adsorption of water (001) and Ca-rich (010), surfaces are found to be energetically favored. The loss of Ca from the surface in exchange for two H is also very favorable. The calculated energies of the various surfaces shed light on the morphologies of HA crystallites found in dissolution studies.

DOI: 10.1103/PhysRevB.78.075427 PACS number(s): 68.35.Dv, 68.43.Bc, 87.85.J−, 71.15.Mb

I. INTRODUCTION

The main mineral component of animal bone[1] is a carbonated form of the naturally occurring mineral, hydroxyapatite [HA, $Ca_{10}(PO_4)_6(OH)_2$]. Along with some other calcium phosphates such as α-tricalcium phosphate, HA is an important biomaterial with applications in bone repair.[2] Natural bone is continually remodeled with some bone cells resorbing bone and others depositing new mineral bone and successful synthetic bone repair materials take part in this remodeling process. Consequently, the scene of the bioactivity of natural bone and of a bone repair material is the interface between the crystalline calcium phosphate and the biological environment, and it is on the solid surface where sites are found for cell attachment.[3] Important features of the HA surface include the surface charge profile, which can be affected by impurity and adsorbate concentrations, dissolution of ions to the aqueous environment, and surface morphology.[4] Recently, surface charge and attachment of proteins on surfaces have been studied using functionalized atomic force microscopy experiments.[5,6] Furthermore, it is possible to engineer HA surfaces at the nanoscale by attaching biologically active molecules.[7] In all of these cases, elucidating the atomistic properties of surfaces is important.

In this work, we model low-index HA surfaces using first-principles methods. The faces studied are the (001), (101), and (010) surfaces, which have multiple geometries depending on the surface cut. To begin with, the surfaces in vacuum are considered, and the reconstructions of the different surfaces are obtained and the surface energies calculated. Next, the effects of H_2O adsorption on the surfaces are studied. Of special interest in this regard is the link between the computational results for surface energies and experimental data concerning the morphologies of HA crystallites in aqueous fluids. Dissolution studies of calcium phosphates in simulated body fluids often lead to the growth of needlelike apatite crystallites elongated along the c axis,[8,9] whereas in natural bone, the HA mineral component is in the form of thin (about $15-40\times250\times500$ Å^3) platelets with large (010) faces and again elongated along the c axis.[10] While the shapes of these crystallites are quite different that the dominantly expressed surfaces are not of $\langle 001\rangle$ type, points to an interesting connection that may have consequences for the biological response, which are worthy of study.

Earlier computational studies of apatite surfaces include calculations of surface energies using empirical shell model potentials to compute minimum energy crystallite shapes.[11] High reactivity of the surfaces, primarily by Ca-O linkages and secondarily by O-H and F-H bondings, was found. While the calculations predicted platelet-shaped crystals for fluoroapatite, similar to those found for the HA mineral component of bone, they predicted (001) as the dominating surface instead of the experimentally observed (010) and do not explain the observed needle-shaped crystallites of HA formed through dissolution. Interactions of hydroxyapatite (001) with water have also been the subject of modeling studies using empirical potentials.[12,13] Zahn and Hochrein[13] reported a layering behavior of water near the surface and Ca-O and PO-H bonds were found, but the OH groups at the surface did not interact strongly with H_2O. However, de Leeuw[12] found dissolution of OH to the fluid. Thus, attention should be paid to the possibility of empirical potentials being unable to describe the delicate O-H chemical bonding and H_2O dissociation. First-principles calculations of the structural properties of bulk apatites including HA were reported by Calderin *et al.*[14] More recently, reports of *ab initio* studies of defect formation in HA[15] and various aspects of the bare (001) surfaces of HA and fluoroapatite[16] (FA) have appeared. Similar first-principles methods have also been used to study charge compensation in carbonate-doped[17] and Si-doped HA.[18] An *ab initio* study of the surface properties of monoclinic α-tricalcium phosphate, an important bone substitute material, has been conducted, including the adsorption of water and some other species.[19] Molecular adsorption of water was found on the (001) surface, but water dissociation was energetically more favorable on the (010) surface, and an attractive interaction was found between two adsorbed water species, which could result in the (010) surface being covered by hydroxyls when water is available.

A Fourier transform infrared spectroscopy study investigating the properties of water adsorbed on HA surfaces has been performed.[20] Absorption bands were assigned to surface PO-H groups that can interact with adsorbed H_2O molecules to form a surface water layer. Adsorption and desorption studies of water on HA surfaces using thermal analysis and

gravimetric techniques have shown the formation of H_2O layers.[4,21–23] It was found that the first monolayer is chemically adsorbed, while additional layers are physisorbed. The results suggest that surface heterogeneities play a role with the most active sites being filled first and the less favorable ones filled afterward with less energy release.[22] FA $[Ca_{10}(PO_4)_6F_2]$ is structurally close to HA. The properties of FA (100) surfaces in water have been studied using high-resolution x-ray reflectivity.[24] The fitting of experimental data to the structural models suggested a Ca- or F-deficient surface and the formation of two water layers. Layering behavior of surface water has also been found for another calcium phosphate phase, brushite $[CaHPO_4 \times 2H_2O]$.[25]

The solvation chemistry of HA has been discussed in Refs. 26–28. Analysis of the phase diagram of calcium phosphates showed that Ca and P in stoichiometric HA do not dissolve congruently, with the solution and the solid having the same Ca/P ratio, because such composition must have a Ca/P ratio below 1.67.[28] Furthermore, depending on the initial Ca/P ratio relative to the congruent point, surface layers may form which have Ca/P ratios smaller or larger than the bulk. An interesting situation to investigate is the dissolution of very small HA crystals so that the surface area to volume ratio is large. In these conditions, the thin surface layer may act as a buffer and the atomistic details of the surface composition become important.[26] In Ref. 29, the dissolution of FA in acidic media was investigated using scanning electron microscopy and Auger electron and infrared spectroscopies. A loss of F and a drop in the Ca/P ratio near the surface took place, suggesting the formation a thin surface layer composed of HPO_4 or H_2PO_4 ions. An atomistic model of dissolution, based on the replacement of F by H_2O, loss of Ca and protonation of surface PO_4 groups was proposed to account for the results. The adsorption and desorption of Ca ions have been studied for HA in electrolyte solutions using surface titration methods.[30] The results indicate that above *p*H =7, increasing the Ca^{2+} concentration of the fluid inhibits the release of Ca^{2+} from the surface. Instead, a Ca^{2+} ion can be adsorbed in exchange for two surface H^+. In a recent study, a combination of experimental and theoretical methods was used to investigate the importance of aqueous media and hydroxyapatite surface reactions in transformation of Si-doped calcium phosphate to apatite.[9]

The aim of this paper is to use *ab initio* modeling to shed light on the atomistic structure of HA surfaces and the interaction of water with these surfaces (Sec. II). The treatment of HA immersed in the fluid is beyond present capabilities, and the present calculation is merely the first step in which the adsorption of the first layer of H_2O molecules on the HA surfaces is considered. It is hoped that this will provide additional foundation for the interpretation of experimental findings. The paper continues with a description of the models used for the surfaces and the computational methods. The results are presented next beginning with the description of surfaces in vacuum, followed by results for H_2O adsorption (Sec. III). In Sec. IV, the results are linked to the experimental data concerning the crystallite morphologies with an explanation for observed large ⟨010⟩ surface areas. Section V completes the paper.

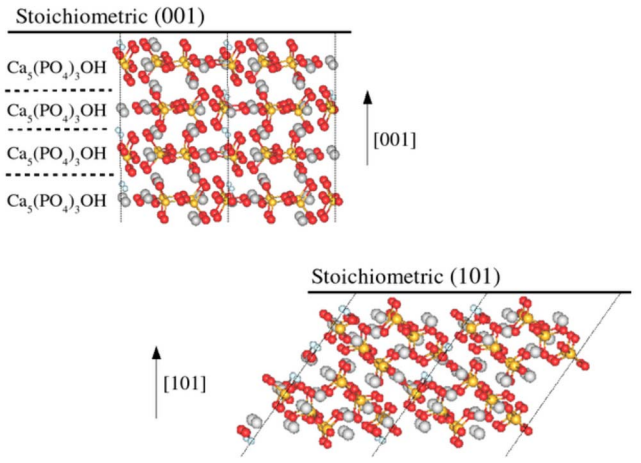

FIG. 1. (Color online) A side view of the stoichiometric (001) and (101) slabs. Multiple unit cells of the periodic structure are shown. The tetrahedral groups are PO_4 ions, the large spheres are Ca atoms, and the small spheres are H atoms. For the (001) surface, the $Ca_5(PO_4)_3OH$ layers have been highlighted. Note the orientation of OH ions in the channel, which breaks the symmetries between the tops and the bottoms of the slabs.

II. SURFACE MODELS AND METHODS

A. Atomistic geometries

Bulk HA has a hexagonal structure, but under certain conditions, it can undergo a phase transformation to monoclinic, in which the unit cell is doubled along the *b* direction with the anion columns alternately reversed (Ref. 23 and citations therein). *Ab initio* studies report that the monoclinic and hexagonal structures have very similar total energies,[14,15] and in order to ease the calculational burden and in common with *ab initio* investigations of defects in HA[15] and the (001) surface of HA,[16] the hexagonal structure of HA, having the smaller unit cell, has been used as the basis of this work. The structure consists of layers of PO_4 groups and Ca ions and of OH ions that occupy channels running along the *c* direction (Fig. 1). The observed lattice parameters are $a=9.42$ Å and $c=6.89$ Å.[23]

Supercells periodic in three dimensions were used in the calculations. Three different surface facets were considered: (010), (001), and (101). The surfaces were modeled using slabs cut from bulk HA so that the crystalline periodicity in the in-plane directions was retained. In the normal direction, the slabs were separated from their periodic images by vacuum layers of 17 Å thick or more, which is enough to make the interaction between the slabs negligible. The model surfaces were constructed so that the slabs were charge neutral. Since the breaking of P-O or O-H bonds is likely to be energetically costly, the surface cuts were chosen so that PO_4 and OH ions were left intact. In the [001] and [010] directions, the structure consists of layers providing natural cuts that maintain charge neutrality (Figs. 1 and 2). In the [001] direction, all these layers have the same stoichiometric composition of $Ca_5(PO_4)_3OH$. Note that because the OH ions are aligned in the [001] direction, there are two slightly different (001) surfaces, depending on the OH orientation. In our slab

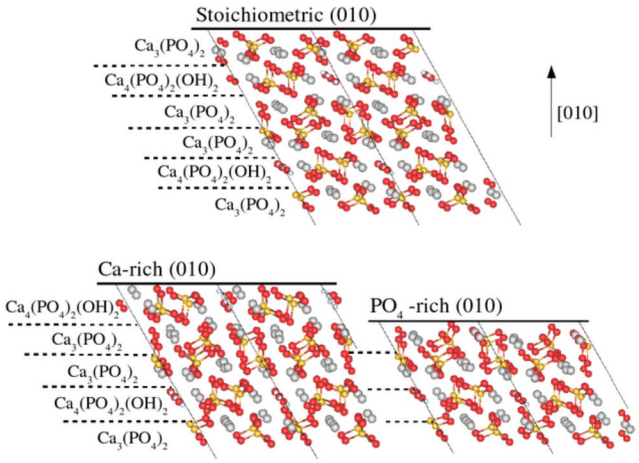

FIG. 2. (Color online) A side view of the (010) surface slabs. Multiple unit cells of the periodic structure are shown. The layered structure has been highlighted.

model, the top and the bottom of the slab have different OH orientations.

For the [010] direction, there are two different types of layers. First, there are *A*-type layers composed of $Ca_3(PO_4)_2$ that have a Ca/P ratio of 1.5 and are therefore PO_4 rich compared to stoichiometric hydroxyapatite with a Ca/P ratio of 1.67. Second, there are *B*-type layers of $Ca_7(PO_4)_2(OH)_2$ that have a Ca/P ratio of 1.75 and are therefore Ca rich. These form the $\cdots AABAAB\cdots$ stacked HA structure so that cutting between the layers yields three chemically distinct terminations (Fig. 2). The $ABA\cdots$ termination is stoichiometric. Removing the outmost *A*-type layer gives $BAA\cdots$ termination, which leaves the slab Ca rich because the PO_4-rich layer has been removed. Finally, removing the Ca-rich *B*-type layer gives $AAB\cdots$ termination and a PO_4-rich slab. These lead to three different (010) surface facets that are denoted stoichiometric, Ca rich, and PO_4 rich, respectively.

Construction of surface slabs began by taking single unit cells of HA that had both the lattice parameter and atomic coordinates relaxed and then stacking these cells in the surface normal direction. The stoichiometric slabs had two HA unit cells stacked in the surface normal direction. The nonstoichiometric (010) surfaces were constructed by starting from the stoichiometric two-cell slab and cleaving off layers from the top of the slab. It is noteworthy that the thicknesses of slabs (10–16 Å) are close to that of natural bone platelets (15–40 Å). On the Ca-rich (010) surface, the topmost Ca atoms can have two different positions; both cases were investigated.

The (101) surface was constructed in a similar way to the other surfaces by cutting a stack of HA unit cells; only one surface cut was found that yielded a stoichiometric charge neutral slab without broken P-O or O-H bonds. With (101), there are again two slightly different surfaces due to two possible OH orientations.

In addition to the bulk HA, a lone H_2O molecule in a large supercell was relaxed to obtain a reference value for calculating water adsorption energies. It is recognized that the localized basis set used in the SIESTA (Ref. 31) software is more appropriate for treating bulk phases, such as ice, than free H_2O molecule. However, when calculating adsorption energies, the free molecule is a more appropriate reference so as to cancel basis set incompleteness errors when calculating the energies of the two. In thermodynamical terms, the lone molecule reference corresponds to low temperature and low vapor density limit. The measured value for the energy per hydrogen bond in ice, 0.29 eV,[32] is adopted as another reference value for the water adsorption energy. In order to perform chemical potential comparisons, as explained below, bulk $Ca(OH)_2$ and β-tricalcium phosphate (Ref. 33 and citations therein) structures were relaxed and their energies calculated.

One limitation of the periodic supercell approach is that the surfaces must remain charge neutral to avoid diverging electrostatic energy. If the HA is immersed in a fluid, the surface charge will depend on the *p*H of the fluid, and therefore, the charge neutrality constraint implies a particular fixed *p*H. However, in recent experiments by atomic force microscopy using functionalized tips, it has been found that pure HA mineral surfaces are close to isoelectric at *p*H=6 with surface charge average of -0.02 C m^{-2} and varying between -0.0037 and -0.072 Cm^{-2}.[5] At most, this implies one unit of negative elementary charge per two or more surface cells. In earlier titration experiments, the point of zero charge for needle-shaped synthetic hydroxyapatite crystallites was determined to be at *p*H=8.5,[8] while in more recent experiments, a value of *p*H=7.3 has been found.[30] In light of this, the charge neutrality constraint represents reasonable physical conditions.

B. First-principles techniques

The total energies and forces were calculated using electron density functional theory as implemented in SIESTA software.[31,34,35] The Perdew–Burke–Ernzerhof generalized gradient functional was used to treat electron exchange and correlation.[36] The Troullier–Martins pseudopotentials[37] that have been reported and used earlier[14] and the Monkhorst–Pack *k*-point grids with reciprocal spacing of 0.8 $Å^{-1}$ or denser were applied.[38] Localized basis sets with double-ζ plus single polarization orbital were used for all valence states, except for Ca 3*p* states and Ca 2*p* semicore states.[39] For the latter two, single-ζ basis sets were used.

C. Geometry optimization methods

In the surface studies, the positions of all atoms in the slabs were relaxed using a conjugate gradients algorithm,[40] while the lattice parameters in the surface plane were held fixed at the calculated bulk values (a=9.36 Å and c =6.99 Å). The supercell dimensions in the directions normal to the surfaces were held fixed at large values, as described above. No symmetry constraints were imposed at any stage. Single H_2O adsorption per cell was studied by placing an H_2O molecule at the surface and relaxing the structure. Different surface sites were investigated: for stoichiometric (001), Ca-rich (010), and PO_4-rich (010), three sites were investigated; and for stoichiometric (010), one site with a prominent dangling O bond. To account for the two possible

OH polarizations, with the (001) and (101) surfaces, the lowest-energy sites were relaxed again with the OH direction reversed in the *c*-axis channel.

The adsorption of two H_2O per cell was studied on stoichiometric (001) and (010) and on Ca-rich (010). With multiple H_2O molecules, the configuration space becomes too large for explicit search through individual configurations. Instead, a simulated annealing[41] was performed. This method can yield configurations that are, if not the actual ground states, physically reasonable low-energy states in which the system has high probabilities to spend time. Of course, the quality of final configurations depends on the annealing rate. The annealing was performed with 1000 K initial and 1 K target temperatures using 1000 time steps of 1 fs each. After the annealing, the final snapshot geometry was taken and the atom positions were relaxed using the conjugate gradients method to remove residual kinetic energy and to find the zero-temperature equilibrium configuration. With the (001) surface, the lowest-energy structure was relaxed again with the OH polarization reversed.

The interesting possibility of the formation of a Ca vacancy (V_{Ca}) in the surface layer[24,29] has also been considered using charge compensation of V_{Ca} by two H that passivate surface PO_4's by forming HPO_4's. This system was studied for Ca-rich (010) and stoichiometric (001) surfaces. In both cases, the outermost Ca ion was removed. For Ca-rich (010), the H atoms were initially placed close to two PO_4 groups so as to form HPO_4 ions. With (001), two initial configurations were considered: two HPO_4 groups or a HPO_4 group and a H_2O ion in the *c*-axis channel.

D. Methods for surface energy comparisons

The challenge for the energy comparisons between the surfaces is that the systems have different chemical compositions and so a direct comparison of calculated supercell energies is uninformative. To overcome this difficulty, we use a chemical potential method where a fictitious external reservoir is used as a source of components so that differences in chemical composition can be treated.[42–44] The cost of this approach is that the surface energies are not uniquely defined but depend on chemical potential variables. However, by imposing equilibrium conditions, the chemical potential can be constrained and the stabilities of surfaces compared.

The surface energy for a slab of stoichiometric composition can be defined as the energy difference between the slab and the equivalent number of bulk formula units, divided by the surface area,

$$S = (E_S - E_B)/A. \tag{1}$$

For the (001) and (101) surfaces, which have two different OH orientations, this formula yields an average.

In order to define the surface energy in nonstoichiometric cases, we assume equilibrium conditions so that the chemical potential of each species of ion is equal to its value in some external reservoir. Thus, the energy to create a surface is the energy difference between the surface slab and the bulk, plus the energy to add or remove ions to reach the correct chemical composition. This chemical potential dependent surface energy can be written as

$$S(\mu[X_1], \ldots, \mu[X_n]) = \left(E_S - \sum_{i=1}^{n} \mu[X_i] \right) \Big/ A, \tag{2}$$

where $\mu[X_i]$ is the chemical potential of ion species X_i, which can be estimated by using chemical potentials of appropriate bulk phases as references. Using bulk HA, this yields

$$\mu[\mathrm{HA}] = 10\mu(\mathrm{Ca}) + 6\mu(\mathrm{PO_4}) + 2\mu(\mathrm{OH}). \tag{3}$$

At $T=0$ K and $p=0$ Pa, the μ(HA) equals E_{HA}: the energy of a bulk hydroxyapatite unit cell.

We often encounter situations where one side of the slab has stoichiometric composition and the other side is nonstoichiometric, and the surface energy of the stoichiometric side is known from an earlier calculation. In these cases, the surface energy contribution from the stoichiometric side is subtracted first.

We denote the surface energies of stoichiometric, Ca-rich, and PO_4-rich (010) surfaces as $S_{S,(010)}$, $S_{\mathrm{Ca},(010)}$ and $S_{P,(010)}$, respectively. Using Eq. (2) for the Ca-rich (010) surface, we find

$$S_{\mathrm{Ca},(010)}(\mu[\mathrm{Ca}], \mu[\mathrm{PO_4}]) = (E_{\mathrm{Ca},(010)} - 2E_{\mathrm{HA}} + 3\mu[\mathrm{Ca}] + 2\mu[\mathrm{PO_4}])/A - S_{S,(010)}, \tag{4}$$

where $E_{\mathrm{Ca},(010)}$ is the energy of the slab and E_{HA} is the energy of a bulk HA unit cell. $S_{S,(010)}$ is subtracted to take into account the other side of the slab that has the stoichiometric composition. Similarly, for the PO_4-rich (010) surfaces, we find

$$S_{P,(010)}(\mu[\mathrm{Ca}], \mu[\mathrm{PO_4}], \mu[\mathrm{OH}]) = (E_{P,(010)} - 2E_{\mathrm{HA}} + 7\mu[\mathrm{Ca}] + 4\mu[\mathrm{PO_4}] + 2\mu[\mathrm{OH}])/A - S_{S,(010)}. \tag{5}$$

This equation can be simplified because the different ions must be in equilibrium with respect to bulk hydroxyapatite; by using Eq. (3), we can write Eq. (5) as

$$S_{P,(010)}(\mu[\mathrm{Ca}], \mu[\mathrm{PO_4}]) = (E_{P,(010)} - E_{\mathrm{HA}} - 3\mu[\mathrm{Ca}] - 2\mu[\mathrm{PO_4}])/A - S_{S,(010)}. \tag{6}$$

Therefore, we can write the surface energies as a function of a single chemical potential variable $3\mu[\mathrm{Ca}] - 2\mu[\mathrm{PO_4}] = \mu[\mathrm{Ca_3(PO_4)_2}]$ for an external reservoir that is in equilibrium with the surface. Because the prefactors of $\mu[\mathrm{Ca_3(PO_4)_2}]$ differ: -1 for Ca-rich (010), $+1$ for PO_4-rich (010), and 0 for stoichiometric surfaces, the relative values of surface energies will depend on this variable. By producing a plot of the surface energies and tracing the lowest-energy envelope, the most stable surfaces can be found. Alternatively, the surface energies can be expressed in terms of a more familiar variable $\mu[\mathrm{Ca(OH)_2}]$, the chemical potential

of $Ca(OH)_2$ by assuming equilibrium with HA and again using Eq. (3).

It is possible to place bounds on the value of $\mu[Ca_3(PO_4)_2]$ in equilibrium conditions by considering appropriate reference systems. The reservoir must be stable with respect to formation of other calcium phosphate phases. Therefore, the $\mu[Ca_3(PO_4)_2]$ of the reservoir must be less than or equal to that of β-tricalcium phosphate (β-TCP)—the low temperature stable phase—leading to a constraint

$$\mu[Ca_3(PO_4)_2] \leq \mu[Ca_3(PO_4)_2]_{\beta\text{-TCP}}. \tag{7}$$

By calculating the total energy of a β-TCP unit cell and dividing by the number of formula units per cell, the $\mu[Ca_3(PO_4)_2]_{\beta\text{-TCP}}$ at zero temperature and pressure can be found. Also, for the surfaces to exist, the HA bulk must itself be stable against decomposition into other phases. Here, we consider the possibility of a decomposition of HA into bulk $Ca(OH)_2$, while $Ca_3(PO_4)_2$ is lost to the reservoir. In order to prevent this from happening, the chemical potential of HA must satisfy a constraint

$$\mu[HA] \leq 3\mu[Ca_3(PO_4)_2] + \mu[Ca(OH)_2]_{\text{bulk}}. \tag{8}$$

The first constraint gives an upper and, for HA surfaces, the second one a lower limit for $\mu[Ca_3(PO_4)_2]$, which provides a window for acceptable values.

We consider the energetics of H_2O adsorption in two ways. First, a simple definition of adsorption energy E_{ads} can be written as

$$E_{\text{ads}} = E_{S+H_2O} - E_S - E_{H_2O}, \tag{9}$$

where E_{S+H_2O} is the energy of the surface with a water molecule, E_S is the energy of the unadorned surface, and E_{H_2O} is the energy of the water molecule, either in some reference phase or in vacuum. Second, in order to compare the surface energies in aqueous environments, it is useful to include the effect of adsorption in the definition of the surface energy so that the surface energy can be written as

$$S(\mu[X_1], \ldots, \mu[X_n]) = \left(E_S - \sum_{i=1}^{n} \mu[X_i] - m\mu[H_2O] \right) \Big/ A. \tag{10}$$

This equation is the generalization of Eq. (2). Here, we have separated the number m of H_2O molecules and the chemical potential, which can be estimated using reference systems, such as an isolated molecule or condensed H_2O phases. This additional variable leads to uncertainties if structures with different amount of water are to be compared.

A subtle point arises if surface energies with adsorbed H_2O are compared in this way: because the area term A may differ from one surface slab to the next, the values are normalized so that the number H_2O of molecules per slab is the same, but the adsorbate coverage per slab area may be different. Because of this complication, the surface energies as a function of H_2O coverage per area will be presented as well as chemical potential plots. For the (001) and (101) surfaces, the slab energies—both with H_2O and in vacuum—were taken as averages over the two OH orientations.

In the case of loss of Ca and adsorption of two H, Eq. (10) can be used again to determine the surface energy as a function of $\mu[Ca_3(PO_4)_2]$. Noting that the Ca vacancy (V_{Ca}) and $2HPO_4$ on the surface can be realized by the exchange

$$2H_2O + 2PO_4 \rightarrow Ca(OH)_2 + V_{Ca} + 2HPO_4, \tag{11}$$

the constraint in Eq. (8) may be used to write $\mu[Ca(OH)_2]$ in terms of $\mu[Ca_3(PO_4)_2]$, leading to an expression for the surface energy for the Ca-rich (010) surface after 2H-Ca exchange,

$$\begin{aligned} S_{2\text{H-Ca},(010)}(\mu[Ca], \mu[PO_4]) &= (E_{2\text{H},(010)} - E_{HA} - 6\mu[Ca] - 4\mu[PO_4] \\ &\quad - 2\mu[H_2O])/A - S_{S,(010)}. \end{aligned} \tag{12}$$

Similarly, for stoichiometric (001), we obtain

$$\begin{aligned} S_{2\text{H-Ca},(001)}(\mu[Ca], \mu[PO_4]) &= (E_{2\text{H},(010)} - E_{HA} - 9\mu[Ca] - 6\mu[PO_4] \\ &\quad - 2\mu[H_2O])/A - S_{S,(001)}. \end{aligned} \tag{13}$$

Again, $S_{S,(010)}$ and $S_{S,(001)}$ take into account the slab geometry where the reaction happens only on the one side. Thus, the surface energies become functions of the familiar chemical potential variable $\mu[Ca_3(PO_4)_2]$: for Ca-rich (010) with a prefactor of −2 and for stoichiometric (001) with a prefactor of −3. Because the $\mu[H_2O]$ carries a prefactor of 2, these equations have the same dependence on water chemical potential as Eq. (10) in the case of adsorption of two H_2O, and these two energies can be compared directly. An average over the two OH polarizations is again taken for the (001) case.

III. RESULTS

We begin the presentation of results by considering clean surfaces in vacuum. These contain undercoordinated O atoms in the surface PO_4 groups that result in dangling bonds. These are a prominent feature of the (010) and (101) surfaces and are of special interest as they provide potential adsorption sites for H_2O. In the (001) surface, these bonds appear partially saturated by neighboring Ca ions. The reactions between H_2O molecules and surfaces are discussed in Sec. III B, where it is found that O-H bonding between the surface PO_4 groups and H_2O molecules plays a critical role in determining the stabilities and atomic structures. Section III C discusses the loss of Ca compensated by two H, which can bind to O atoms in the surface and saturate dangling bonds.

A. Surfaces in vacuum

1. Surface energies

When the surface energies are plotted as a function of $\mu[Ca_3(PO_4)_2]$ (Fig. 3), the stoichiometric (001) is found to have the lowest energy over a wide range of chemical potential, although this value is somewhat higher than the 0.054 $eV/Å^2$ value reported by Rulis *et al.*[16] calculated us-

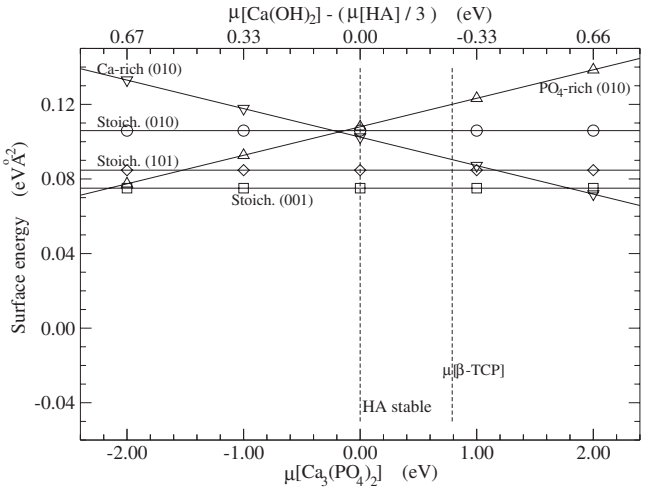

FIG. 3. The surface energies as a function of $Ca_3(PO_4)_2$ chemical potential in vacuum: squares, stoichiometric (001); circles, stoichiometric (010); diamonds, stoichiometric (101); up triangles, PO_4-rich (010); and down triangles, Ca-rich (010). For the (001) and (101) surfaces, the energy is the average over two OH polarizations. The top x axis shows the corresponding $Ca(OH)_2$ chemical potential, calculated using Eq. (3).

ing different methods. At high values of $\mu[Ca_3(PO_4)_2]$, the Ca-rich (010) becomes favorable, while at low values, the PO_4-rich (010) is favored. However, the range of values where these nonstoichiometric surfaces are stable is outside the window of stability defined by bulk HA, $Ca(OH)_2$, and β-TCP. The stoichiometric (010) and (101) surfaces always have higher energies than stoichiometric (001). The lower energy of the (001) may be related to the coordination of O atoms in the top layer, as discussed in Sec. III A 2.

2. Atomic structure

The (001) surface showed only minor relaxation with the dominant effect being a collective motion of ions in the normal direction, probably to reduce the surface electric dipole. For example, the distance between the outermost Ca layer and the next Ca-P layer decreased to 1.3–1.4 Å from the bulk HA value of 1.7 Å. The changes in P-O bond lengths were relatively small. The relaxed stoichiometric (010) and (101) surfaces exhibited a larger spread of P-O bond lengths than the bulk HA. No clear trends were found, except that on the (010) surface the P-O bonds pointing away from the surface layer toward the bulk were all elongated to 1.61–1.63 Å. Similar features were found on the nonstoichiometric (010) surfaces with P-O bond lengths of 1.54–1.66 Å. The top OH groups on the (101) surface underwent about 90° rotation to become oriented perpendicular to the c channel direction so that the outermost surface layers are close to symmetry equivalent.

B. Surface-water interactions

1. Adsorption energies

The results for H_2O adsorption energies are given in Table I. For a single H_2O molecule per cell, the adsorption energies on the (010) surfaces, at about 2.7–3.0 eV, are the largest and indicate chemisorption. On the stoichiometric (001), the adsorption energy is lower, 1.8 eV. This difference has the effect of narrowing the range of stability for the stoichiometric (001) surface and bringing the surface energies closer to one another so that those of stoichiometric (010) and (001) differ little (Fig. 4). Both the stoichiometric (001) and Ca-rich (010) now fall into the window of stability relative to bulk HA, $Ca(OH)_2$, and β-TCP. However, the PO_4-rich (010) is still energetically unfavorable. Table I shows that on the stoichiometric (101) the H_2O binding is weaker than on (010) surfaces. The cases of the PO_4-rich (010) and the (101) sur-

TABLE I. Adsorption energies of H_2O molecules. For the (001) and (101) surfaces, the values for the two kinds of surface with different OH polarization directions are given. (+) indicates polarization in which the H are closer to the surface where adsorption takes place, while (–) is the opposite.

Surface	Number of H_2O	Adsorption energy/H_2O (eV)
(001), (+)	1	1.77
(001), (–)	1	1.75
(001), (+)	2	1.79
(001), (–)	2	1.80
(010) stoichiometric	1	3.04
	2	2.60
(010) Ca rich	1	2.69
	2	2.51
(010) PO_4 rich	1	2.83
(101) (+)	1	1.97
(101) (–)	1	1.97

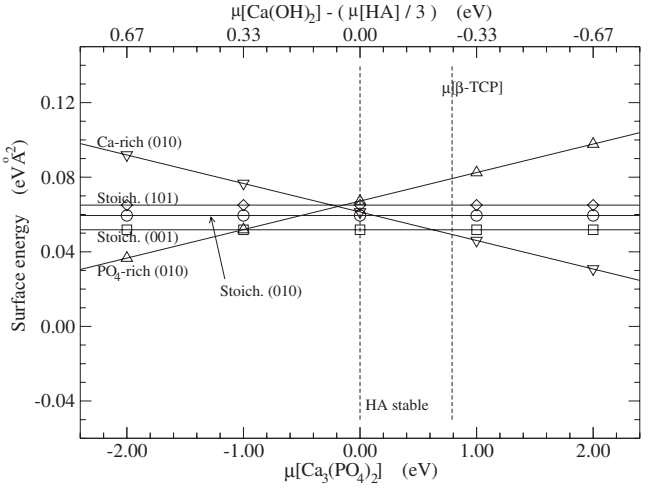

FIG. 4. The surface energies as a function of $Ca_3(PO_4)_2$ chemical potential after adsorption of a single H_2O: squares, stoichiometric (001); circles, stoichiometric (010); diamonds, stoichiometric (101); up triangles, PO_4-rich (010); and down triangles, Ca-rich (010). For the (001) and (101) surfaces, the energy is the average over two OH polarizations. The top x axis shows the corresponding $Ca(OH)_2$ chemical potential, calculated using Eq. (3).

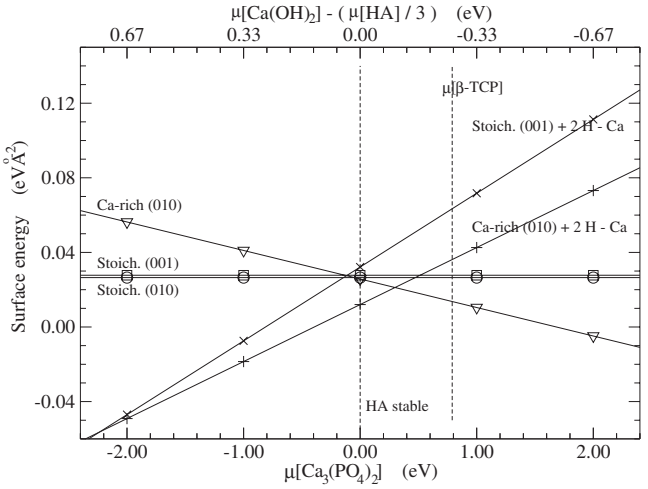

FIG. 5. The surface energies as a function of $Ca_3(PO_4)_2$ chemical potential after adsorption of two H_2O or after exchange of two H for Ca: squares, stoichiometric (001)+2H_2O; circles, stoichiometric (010)+2H_2O; down triangles, Ca-rich (010)+2H_2O; pluses, Ca-rich (010)+2H−Ca; and crosses, stoichiometric (001)+2H−Ca. For the (001) surface, the energy is the average over two OH polarizations. The top x axis shows the corresponding $Ca(OH)_2$ chemical potential, calculated using Eq. (3).

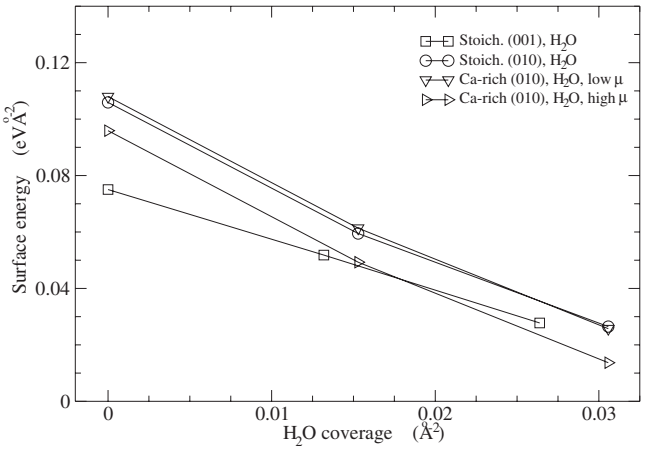

FIG. 6. The relative surface energies as a function of H_2O coverage for 0–2 molecules per cell: the lines are merely to guide the eye. Results for stoichiometric (001) and (010) surfaces and for the Ca-rich (010) surface are shown. The surface energy of the Ca-rich (010) surface is a function of the chemical potential $\mu[Ca_3(PO_4)_2]$, and for this case, two graphs are shown corresponding to the lowest and highest values of this μ at the HA stability window. In all the cases, a lone H_2O molecule was used to determine the H_2O chemical potential.

faces were not investigated further. The effect of the channel OH direction on the adsorption energies on the (001) and (101) surfaces was found to be very small.

The addition of a second H_2O further enhanced the trends seen with single H_2O adsorption. (Fig. 5) The energy of the Ca-rich (010) surface was lowered even more relative to the (001) surface. Interestingly, the adsorption energy of the second H_2O on the stoichiometric (010) surface decreased substantially, indicating that the sites remaining after single H_2O adsorption are less active. The surface energies as a function of H_2O coverage are shown in Fig. 6. The crossover from (001) to Ca-rich (010) being the most stable takes place at coverages of about one H_2O per unit area depending on the $\mu[Ca_3(PO_4)_2]$. The figure shows the results obtained using the H_2O molecule reference system. With ice as the reference system, the surface energies decrease a little less steeply.

2. Atomic geometries

The typical pattern of H_2O adsorption on HA surfaces was the formation of a bond between O of H_2O and Ca and H-O bonds of different strengths between the molecule and PO_4 ions in the surface layer. A single H_2O per cell on the stoichiometric (010) surface illustrated in Fig. 7(a), for which the adsorption energy was largest, was the exception with dissociative adsorption into OH and HPO_4 taking place, but the products remained close with a HO-HPO_4 distance of 1.75 Å. For the (010) surfaces visualized in Figs. 8(a) and 9, the stronger binding compared to (001) is reflected in shorter H-O bond lengths between surface PO_4 groups and the single H_2O. Bond lengths are listed in Table II. On the (001) surface, displayed in Fig. 10, the H_2O formed OH bonds with the surface O in the second layer, and the O of the H_2O bonded with a second layer Ca. On the (101) surface shown in Fig. 11 the relaxed H_2O had two shorter O-H bonds to surface PO_4 groups and one longer bond between the surface OH group and the water O atom.

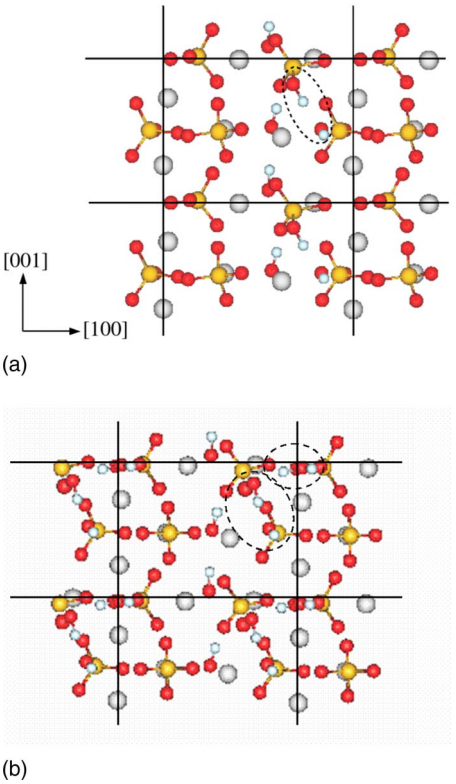

FIG. 7. (Color online) A top view of the stoichiometric (010) surface after (a) one and (b) two H_2O (circled) adsorption and dissociation. Atoms below the surface have been removed for clarity, and multiple unit cells of the periodic structure are shown.

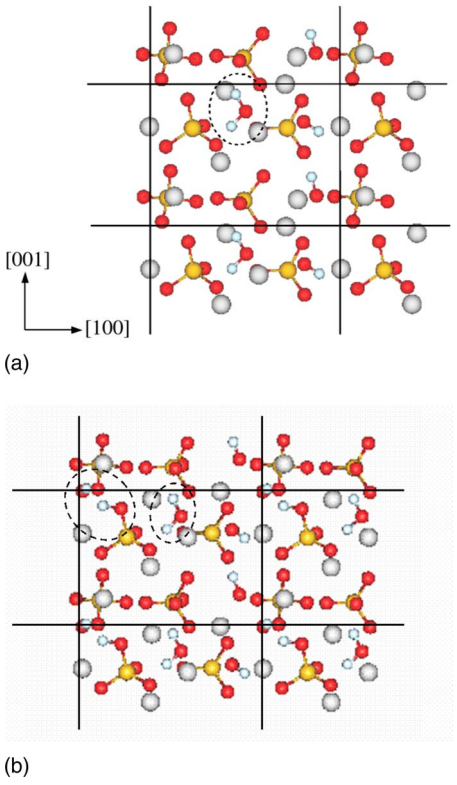

FIG. 8. (Color online) A top view of the Ca-rich (010) surface after (a) one and (b) two H_2O (circled) adsorption. Atoms below the surface have been removed for clarity, and multiple unit cells of the periodic structure are shown.

The stoichiometric and the Ca-rich (010) surfaces with two adsorbed water molecules per cell are illustrated in Figs. 7(b) and 8(b), respectively. On the Ca-rich (010) surface, an interesting linkage between a PO_4 ion and the second H_2O was observed. The H-O bond in the water molecule was substantially elongated to 1.38 Å, while the PO-H bond length was 1.10 Å so that the H_2O was close to dissociation with a small energy barrier. The other H in this water molecule pointed toward the vacuum, whereas the first molecule was flat on the surface. On the stoichiometric (010), both H_2O had an OH pointing out of the surface. The first H_2O remained dissociated with the OH and HPO_4 products still in close contact. The second H_2O formed a single H-O bond with a PO_4, and the water O was bonded to two Ca's. On the (001) surface, which is not illustrated, only one O-H linkage in the top O layer was detected, the two water molecules again preferring to bond to Ca and O in the second layer.

TABLE II. The O-H distances between PO_4 groups and H_2O molecules. As in Table I, (+) and (−) indicate the direction of the OH polarization on the surface where the adsorption takes place.

Surface	Number of H_2O	O-H distance (Å)
(001), (+)	1	1.78, 1.86
(001), (−)	1	1.80, 1.85
(001), (+)	2	1.85, 1,89; 1.75, 2.29
(001), (−)	2	1.84, 1,97; 1.74, 2.31
(010) stoichiometric	1	Dissociated
	2	Dissociated; 1.65
(010) Ca rich	1	1.52, 1.67
	2	1.60, 1.67; 1.10
(010) PO_4 rich	1	1.64, 1.77
(101) (+)	1	1.70, 1.95
(101) (−)	1	1.70, 2.02

C. Calcium loss

The Ca loss in exchange for two H (+2H−Ca) was studied on the stoichiometric (001) and Ca-rich (010) surfaces and was found to be very favorable energetically. Since the reaction leads to a highly Ca-deficient surface, the reaction energy depends strongly on $\mu[Ca_3(PO_4)_2]$, but at $\mu[Ca_3(PO_4)_2]=0$, it was much favored on both surfaces. On the (001) surface, there was some asymmetry between the two OH polarization directions and the reaction was more favorable by 0.25 eV on the (−)-oriented side. The plots of surface energies in Fig. 5 show that the Ca-rich (010) (+2H−Ca) surface competes with the Ca-rich (010) plus $2H_2O$ as the most stable surface in the HA stability window.

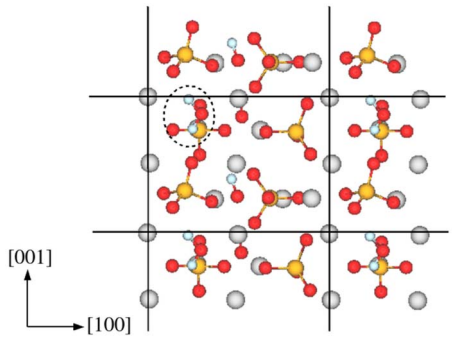

FIG. 9. (Color online) A top view of the PO_4-rich (010) surface after H_2O (circled) adsorption. Atoms below the surface have been removed for clarity, and multiple unit cells of the periodic structure are shown.

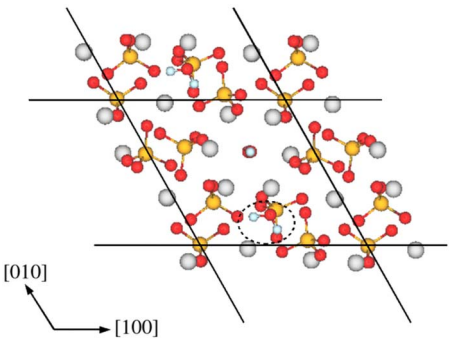

FIG. 10. (Color online) A top view of the stoichiometric (001) surface after H_2O (circled) adsorption and dissociation. Atoms below the surface have been removed for clarity, and multiple unit cells of the periodic structure are shown.

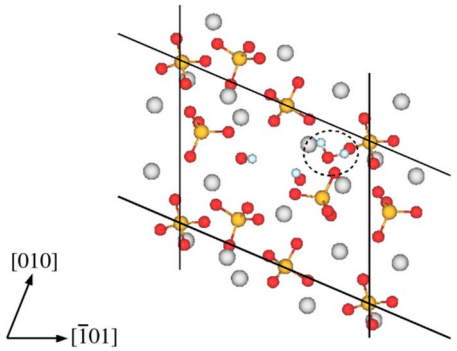

FIG. 11. (Color online) A top view of the stoichiometric (101) surface after H_2O (circled) adsorption and dissociation. Atoms below the surface have been removed for clarity, and multiple unit cells of the periodic structure are shown.

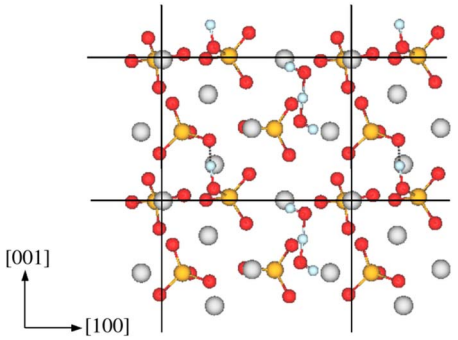

FIG. 12. (Color online) A top view of the Ca-rich (010) surface after 2H addition and Ca removal. Atoms below the surface have been removed for clarity, and multiple unit cells of the periodic structure are shown.

On the Ca-rich (010) surface, the structure, which initially had two HPO_4 groups, relaxed into a PO_4-H-O_4P complex and a HO-H-OH, as shown in Fig. 12. This resulted from a H jumping from a PO_4 to one of the OH groups, while the original H in the O-H group relaxed so as to link the two channel OH's. The H-(OH) distances were 1.17 and 1.27 Å. The other H was shared by two surface PO_4 groups with bond lengths of 1.14 and 1.29 Å. The reaction energy for extracting an H_2O unit from the channel was also calculated, but this process was found to be very unfavorable with an energy cost of 3.08 eV.

On the stoichiometric (001) (+2H−Ca) surface, the formation of O-H-O bonds between neighboring surface PO_4 groups was observed. These bonds formed between surface O's and O's in the second layer. The lengths of the surface O-H bonds were 0.98–1.00 Å, while the bonds between H and O's in the second layer were longer: 1.79 and 1.84 Å on the (−)-polarized surface and 1.81 and 1.94 Å on the (+)-polarized surface. In contrast to the Ca-rich (010) surface, the formation of an H_2O unit from the added H and a channel OH was energetically unfavorable. When this complex was taken as an initial configuration, it spontaneously dissociated into OH and HPO_4 during the relaxation.

IV. DISCUSSION

In vacuum, the HA surfaces were characterized by undercoordinated O atoms in surface PO_4 groups. An important mechanism for water adsorption was bonding between these O atoms and H_2O molecules via H. Details of the atomic structure of the surfaces lead to different strengths of adsorption, and in one case—the stoichiometric (010) surface—dissociative adsorption was observed. This H_2O adsorption behavior is similar to that found in an earlier modeling study of α-tricalcium phosphate surfaces.[19] These results highlight the importance of an accurate description of the making and breaking of O-H bonds when modeling calcium phosphate surfaces.

In order to estimate the hydrophilic character of HA surfaces, it is illuminating to compare the adsorption energy of an H_2O molecule with the cohesive energy of condensed H_2O phases with well-coordinated hydrogen bond networks. One way of making such a comparison is to use cubic ice as a reference phase. The lone H_2O molecule and ice represent extremes; in the former, the lone pair electrons of O are nonbonded, while in the latter, a fully coordinated network forms. For ice, the measured calculated energy per hydrogen bond is 0.29 eV,[32] which is about 1/10 of the single molecule E_{ads} on the (010) surface and about 1/6 of E_{ads} on the (001) surface. This indicates that if the surfaces are brought into contact with water, the energy gained by water-surface interaction is more substantial on the (010) compared to the energy cost for defect creation by breaking a bond in the water H-bond network, and therefore, it is more hydrophilic. This may have interesting consequences on the crystallization of HA and biological activity on different facets.

Surface heterogeneity as a cause for higher adsorption energies at the initial stages of H_2O adsorption was discussed in Ref. 22. In the experiments, the cross-sectional area of the adsorbed H_2O was determined to be 11.5 $Å^2$, or 5–9 molecules per surface unit cell at monolayer coverage, depending on the surface plane. Because of surface heterogeneities, the adsorption energy of the first 1–2 H_2O is likely to be higher that the average adsorption energy at the full monolayer coverage, as the first molecules occupy the most active sites. This effect of decreasing adsorption energy is already seen for two H_2O on the stoichiometric (010), where the adsorption energy was found to decrease by 0.44 eV from the value with single H_2O adsorption (Table I). With two H_2O molecules on the Ca-rich (010), one of the water hydrogens pointed toward the vacuum; such hydrogens have been proposed to act as binding sites for the H_2O molecules in the second monolayer.[21]

On the (001) surfaces, the *c* channel OH groups played a minor role in the adsorption of water with the adsorption energy being almost independent of the direction of their polarization. The OH's are in the channel, surrounded by Ca ions, which shield them from adsorbed H_2O. Also, on the stoichiometric and PO_4 rich (010) surfaces, the OH's were buried in the slab and not exposed to adsorbed molecules. However, this was not the case on the Ca-rich (010) surfaces where the OH's would react with H atoms when Ca was removed.

The (010) surfaces are much more reactive than the (001) surfaces. This may have an interesting connection to the ob-

servation that bone platelets preferentially express (010) surfaces; it may be that the high reactivity affects the biological activity in yet unknown ways, and therefore, the body preferably synthesizes thin platelets. Also, this may provide clues to the kinds of crystal morphologies that would provide optimal biological activity in artificial HA.

The reaction in which Ca is lost in exchange for two H is energetically favorable. Such a charge compensation mechanism is supported by infrared spectroscopy results for surfaces of Ca-deficient HA.[20] Our calculations qualitatively support the proposal of Ca desorption being the driving mechanism for dissolution;[30] if the chemical potential of Ca was increased, the reaction would become less favorable and could even be reversed as is seen when Ca is added to the electrolyte in Ref. 30. This mode of Ca dissolution applies to the atomistically thin outer surface layer in contrast to the formation of macroscopic Ca-deficient HA layers by incongruent dissolution.[28] Consequently, Ca release by the Ca-H exchange should be most influential in HA samples with large surface-to-volume ratio, such as fine powders and porous systems. This Ca-H reaction mechanism is less favorable on the (001) than on the (010) surface, which may have interesting consequences, because if the Ca release to the aqueous environment from (001) is reduced, the surfaces will have different chemical properties.

The stoichiometric (010) has been proposed as the expressed HA surface in Ref. 30 [the (200) in their notation]. This proposal is based on geometry considerations for adsorption of Ca^{2+} ions. Our results indicate that this surface is unstable, either compared to (001), Ca-rich (010), or Ca-H exchanged Ca-rich (010). One possible explanation for this disagreement is that the geometric model used in Ref. 30 did not include the surface relaxation effects, which are prominent on Ca-H exchanged Ca-rich (010). Furthermore, both our results and those in Ref. 30 indicate that the surface morphology is very sensitive to chemical environment, and therefore, HA surfaces do not have a unique favored facet.

The Ca-2H exchange process forms one step in the dissolution reaction sequence proposed in Ref. 29. The initial step in this sequence is an exchange of channel OH^- for H_3O^+, the second step is a loss of Ca^{+2} from the positively charged surface, and the third is the Ca-2H exchange where $CaHPO_4$ complexes are formed. Finally, the $CaHPO_4$ dissolves as Ca^{2+} and phosphate anions. Our results for the reaction energetics imply that the Ca-2H exchange plays an important role in the dissolution. Furthermore, the results suggest that the initial stage involving adsorbed H_3O^+ should be very short-lived because of the affinity of surface PO_4 groups for protons would cause the reaction to proceed rapidly toward the formation of HPO_4 groups and Ca desorption. Again, the atomistic details of the surfaces are important. On the Ca-2H exchanged (001) surface, two HPO_4 groups were formed, while on the corresponding Ca-rich (010) surface, the adsorbed H's tended to form linkages between the PO_4 groups, and a PO_4 and a surface OH. Interestingly, on the (001) surface, a H_2O in the *c*-directed channel was unfavorable, while on the Ca-rich (010) surface, the atomic geometry could be interpreted as a H_2O interacting strongly with the remaining channel OH and a surface PO_4.

V. CONCLUSIONS

Different hydroxyapatite surfaces, H_2O adsorption, and Ca loss were studied using first-principles simulations. In vacuum, the (001) surface is the most stable. The results for H_2O adsorption show that all the surfaces react strongly with water because of exposed undercoordinated O atoms. The (010)-type surfaces were found to be the most reactive while (001) was the least reactive with H_2O. After adsorption of a single H_2O per cell, both (001) and Ca-rich (010) surfaces were stable, depending on the chemical environment. Wulff plots using the calculated surface energies suggest that the equilibrium shape of an HA crystallite changes systematically as water is adsorbed. The surface energy of the (010) face decreases with respect to that of the (001), and the (010) faces become more exposed as the number of adsorbed H_2O molecules increases. The Ca-rich (010) face is of particular interest. At the HA edge of the stability window, the surface energy of this face is seen to be very similar to that of the stoichiometric (010) face, but at the other β-TCP edge, the surface energy is much lower so that for two adsorbed H_2O, the equilibrium crystallite is elongated along the *c* axis with an aspect ratio of about 2. This may be related to the morphology of HA crystallites grown in aqueous media, and, perhaps, also to the nature of the HA platelets found in natural bone. Ca loss in exchange for two H was very favorable energetically. The ion release may have interesting consequences on the bioactivity. The identification of stable surface structures and the role of H_2O adsorption give a promising starting point for future investigations, such as the studies of impurities and adsorption of different molecules.

ACKNOWLEDGMENTS

The support of the NSERC and Millenium Biologix Corp. is gratefully acknowledged. R.A. also acknowledges the hospitality of E. Kaxiras of Department of Physics, Harvard University.

*Present address: Interactive Supercomputing, Inc; astala@physics.queensu.ca
†stott@mjs.phy.queensu.ca

[1] J. C. Elliott, *Structure and Chemistry of the Apatites and Other Calcium Orthophosphates* (Elsevier, Amsterdam, 1994).
[2] S. V. Dorozhkin and M. Epple, Angew. Chem., Int. Ed. **41**, 3130 (2002).
[3] P. Ducheyne and Q. Qiu, Biomaterials **20**, 2287 (1999).
[4] A. S. Posner, J. Biomed. Mater. Res. **19**, 241 (1985).
[5] J. Vandiver, D. Dean, N. Patel, W. Bonfield, and C. Ortiz, Biomaterials **26**, 271 (2005).
[6] A. M. Pietak and M. Sayer, Biomaterials **27**, 3 (2006).

[7] A. J. García, Biomaterials **26**, 7525 (2005).
[8] L. C. Bell, A. M. Posner, and J. P. Quirk, J. Colloid Interface Sci. **42**, 250 (1973).
[9] L. Tuck, R. Astala, J. Reid, M. Sayer, and M. J. Stott, J. Mater. Sci.: Mater. Med. **19**, 917 (2008).
[10] S. Weiner and W. Traub, FASEB J. **6**, 879 (1992).
[11] D. Mkhonto and N. H. de Leeuw, J. Mater. Chem. **12**, 2633 (2002).
[12] N. H. de Leeuw, Phys. Chem. Chem. Phys. **6**, 1860 (2004).
[13] D. Zahn and O. Hochrein, Phys. Chem. Chem. Phys. **5**, 4004 (2003).
[14] L. Calderín, M. J. Stott, and A. Rubio, Phys. Rev. B **67**, 134106 (2003).
[15] K. Matsunaga and A. Kuwabara, Phys. Rev. B **75**, 014102 (2007).
[16] P. Rulis, H. Yao, L. Ouyang, and W. Y. Ching, Phys. Rev. B **76**, 245410 (2007).
[17] R. Astala and M. J. Stott, Chem. Mater. **17**, 4125 (2005).
[18] R. Astala, L. Calderín, X. Yin, and M. J. Stott, Chem. Mater. **18**, 413 (2006).
[19] X. Yin and M. J. Stott, J. Chem. Phys. **124**, 124701 (2006).
[20] T. Ishikawa, M. Wakamura, and S. Kondo, Langmuir **5**, 140 (1989).
[21] M. E. Dry and R. A. Beebe, Science **64**, 1300 (1960).
[22] H. M. Rootare and R. G. Craig, J. Dent. Res. **56**, 1437 (1977).
[23] M. Markovic, B. O. Fowler, and M. S. Tung, J. Res. Natl. Inst. Stand. Technol. **109**, 553 (2004).
[24] C. Park, P. Fenter, Z. Zhang, L. Cheng, and N. C. Sturchio, Am. Mineral. **89**, 1647 (2004).
[25] J. Arsic, D. Kaminski, P. Poodt, and E. Vlieg, Phys. Rev. B **69**, 245406 (2004).
[26] A. N. Smith, A. S. Posner, and J. P. Quirk, J. Colloid Interface Sci. **48**, 442 (1974).
[27] S. Chander and D. W. Fuerstenau, J. Colloid Interface Sci. **70**, 506 (1979).
[28] P. W. Brown and R. I. Martin, J. Phys. Chem. B **103**, 1671 (1999).
[29] S. V. Dorozhkin, J. Colloid Interface Sci. **191**, 489 (1997).
[30] I. S. Harding, N. Rashid, and K. A. Hing, Biomaterials **26**, 6818 (2005).
[31] P. Ordejón, E. Artacho, and J. M. Soler, Phys. Rev. B **53**, R10441 (1996).
[32] E. Whalley, Trans. Faraday Soc. **53**, 1578 (1957).
[33] X. Yin, M. J. Stott, and A. Rubio, Phys. Rev. B **68**, 205205 (2003).
[34] P. Hohenberg and W. Kohn, Phys. Rev. **136**, B864 (1964).
[35] W. Kohn and L. Sham, Phys. Rev. **140**, A1133 (1965).
[36] J. P. Perdew, K. Burke, and M. Ernzerhof, Phys. Rev. Lett. **77**, 3865 (1996).
[37] N. Troullier and J. L. Martins, Phys. Rev. B **43**, 1993 (1991).
[38] H. J. Monkhorst and J. D. Pack, Phys. Rev. B **13**, 5188 (1976).
[39] E. Artacho, D. Sánchez-Portal, P. Ordejón, A. García, and J. M. Soler, Phys. Status Solidi B **215**, 809 (1999).
[40] M. S. Bazaraa, H. D. Sherali, and C. M. Shetty, *Nonlinear Programming: Theory and Algorithms* (Wiley, USA, 1993).
[41] S. Kirkpatrick, C. D. Gelatt, and M. P. Vecchi, Science **220**, 671 (1983).
[42] E. Kaxiras, K. C. Pandey, Y. Bar-Yam, and J. D. Joannopoulos, Phys. Rev. Lett. **56**, 2819 (1986).
[43] E. Kaxiras, Y. Bar-Yam, J. D. Joannopoulos, and K. C. Pandey, Phys. Rev. B **35**, 9625 (1987).
[44] D. B. Laks, C. G. Van de Walle, G. F. Neumark, and S. T. Pantelides, Phys. Rev. Lett. **66**, 648 (1991).